Superior Electrocatalytic Hydrogen Evolution at Engineered Non-Stoichiometric Two-Dimensional Transition Metal Dichalcogenide Edges

Journal:	*Journal of Materials Chemistry A*
Manuscript ID	TA-ART-05-2019-005546.R1
Article Type:	Paper
Date Submitted by the Author:	05-Jul-2019
Complete List of Authors:	Hu, Guoxiang; Oak Ridge National Laboratory, Center for Nanophase Materials Sciences Fung, Victor; Oak Ridge National Laboratory, Center for Nanophase Materials Sciences Sang, Xiahan; Oak Ridge National Laboratory, Center for Nanophase Materials Science Unocic, Raymond; Oak Ridge National Laboratory, Center for Nanophase Materials Sciences Ganesh, Panchapakesan; Oak Ridge National Laboratory,

Superior Electrocatalytic Hydrogen Evolution at Engineered Non-Stoichiometric Two-Dimensional Transition Metal Dichalcogenide Edges

Guoxiang Hu*, Victor Fung, Xiahan Sang, Raymond R. Unocic, and P. Ganesh*
hug1@ornl.gov, ganeshp@ornl.gov
Center for Nanophase Materials Sciences, Oak Ridge National Laboratory, Oak Ridge,
Tennessee 37831, US

Abstract:

Two-dimensional transition metal dichalcogenide (TMDC) edges show activity for catalytic hydrogen evolution reaction (HER), but further improvements require extrinsic doping, usually performed in an Edisonian manner. Herein we ask if tuning the non-stoichiometric degree of the edges itself can improve HER activities. Using first-principles density functional theory (DFT), we study six non-stoichiometric $MoSe_2$ edges that have been recently synthesized under a scanning transmission electron microscope (STEM). We find that non-stoichiometric edges can have near optimal HER activity over the conventional stoichiometric edges. More excitingly, we find a strong linear correlation between Bader charges on H and the Gibbs free energy of hydrogen adsorption (ΔG_H) at these edges, providing a design principle for discovering better HER catalytic edges. In general, HER activity is not only influenced by the formation of H-Se/Mo chemical bonds as previously thought, but also by geometric reconstructions and charge redistribution. Our predictions open the door for engineering non-stoichiometric TMDC edges for superior HER activity.

Introduction

The electrochemical hydrogen evolution reaction (HER) using renewable energy can provide a sustainable supply of fuel for future societies with hydrogen as a key energy carrier.[1] To date, Pt-based materials remain the most efficient electrocatalysts for HER.[2] However, the low natural abundance and high cost of Pt hampers its widespread use at the industrial scale. Thus, it is highly desirable to develop efficient, low-cost and earth-abundant electrocatalysts for HER.[3-7]

Among the earth-abundant materials, two dimensional (2D) transition metal dichalcogenides (TMDCs) have been gaining widespread attention for the design of novel HER catalysts.[8-12] Normally, the edges of 2D TMDC are responsible for the HER activities.[13, 14] Unfortunately, further improvements of the activities of the edges require extrinsic doping, usually performed in an Edisonian manner.[15-20] Therefore, an urgent question is if tuning the degree of non-stoichiometry at the edges itself can improve the catalytic activity, as the non-stoichiometric materials often show dramatically different properties compared to their stoichiometric counterparts.

Recently, *in situ* heating experiments using scanning transmission electron microscopy (STEM) to track the edge evolution in monolayer $Mo_{1-x}W_xSe_2$ ($x = 0.05$) flakes demonstrated that by varying the local chemical environment, a variety of reconstructed non-stoichiometric edges can be formed.[21] We study the HER activities of these non-stoichiometric $MoSe_2$ edges, and compare them with the conventional stoichiometric edges (ZZSe and ZZMo) by using first-principles density functional theory (DFT). Our goal is to find out if tuning the non-stoichiometry degree of the edges can improve their HER activity, and explain the origin of these changes.

Results and discussion

Energetics and structures of H adsorption on the reconstructed non-stoichiometric edges

The edges are labeled based on the orientation with respect to the hexagonal lattice of $MoSe_2$ (e.g., Se-oriented ZZSe, and Mo-oriented ZZMo) and the outermost termination group (e.g., Se-terminated (-Se), and nanowire-terminated (-NW)). By calculating μ_{Mo}-dependent formation energies, Sang, et al. have shown that six reconstructed non-stoichiometric edges ZZSe-Mo-NW30, ZZMo-NW30, ZZSe-Se, ZZMo-Se2, ZZSe-GB4-Se , and ZZMo-Se (Fig 1) are the most stable edge structures for a specific chemical environment (have the lowest formation energies within their respective μ_{Mo} window). This is also confirmed by their experimental observations.[21]

To understand the stability of the non-stoichiometric edges under HER condition, we have calculated the edge free energies, and compared them with the stoichiometric edges (Table 1) by using the methods reported by Nørskov group.[22-24] As one can see, for the Mo-orientated edges, all the non-stoichiometric edges are more stable than the stoichiometric ZZMo edge, while for the Se-orientated edges, only ZZSe-GB4-Se is more stable than ZZSe. It is noted that among the eight edges, ZZMo is the most unstable one. However, it has been shown that ZZMo can be stabilized under Mo-rich conditions, and plays important roles in the catalytic and magnetic properties.[25-27] For example, atomic-resolution electron microscopy imaging has revealed that nanoporous MoS_2 films grown under Mo-rich conditions using molecular beam epitaxy (MBE) contain large numbers of Mo-terminated edges, and the percentage of ZZMo is as high as 44.0%. Moreover, attributed to the presence of large quantity of ZZMo, the nanoporous MoS_2 films showed improved HER activity.[27] This indicates that ZZMo edge can be synthesized under Mo-rich conditions, and kinetically stabilized under the HER condition. Since ZZSe-Se and ZZSe-Mo-MW30 both have lower edge free energies than ZZMo, it is believed that they can also be kinetically stabilized under the HER condition.

Table 1 Edge free energies (eV/nm) of the six non-stoichiometric edges and two stoichiometric edges under HER conditions.

	ZZSe-Se	**ZZSe-Mo-MW30**	**ZZSe-GB4-Se**	**ZZSe**
Se-orientated	1.7253	1.6970	1.4394	1.5288
	ZZMo-Se2	**ZZMo-Se**	**ZZMo-NW30**	**ZZMo**
Mo-orientated	1.5004	1.2735	1.6191	1.7602

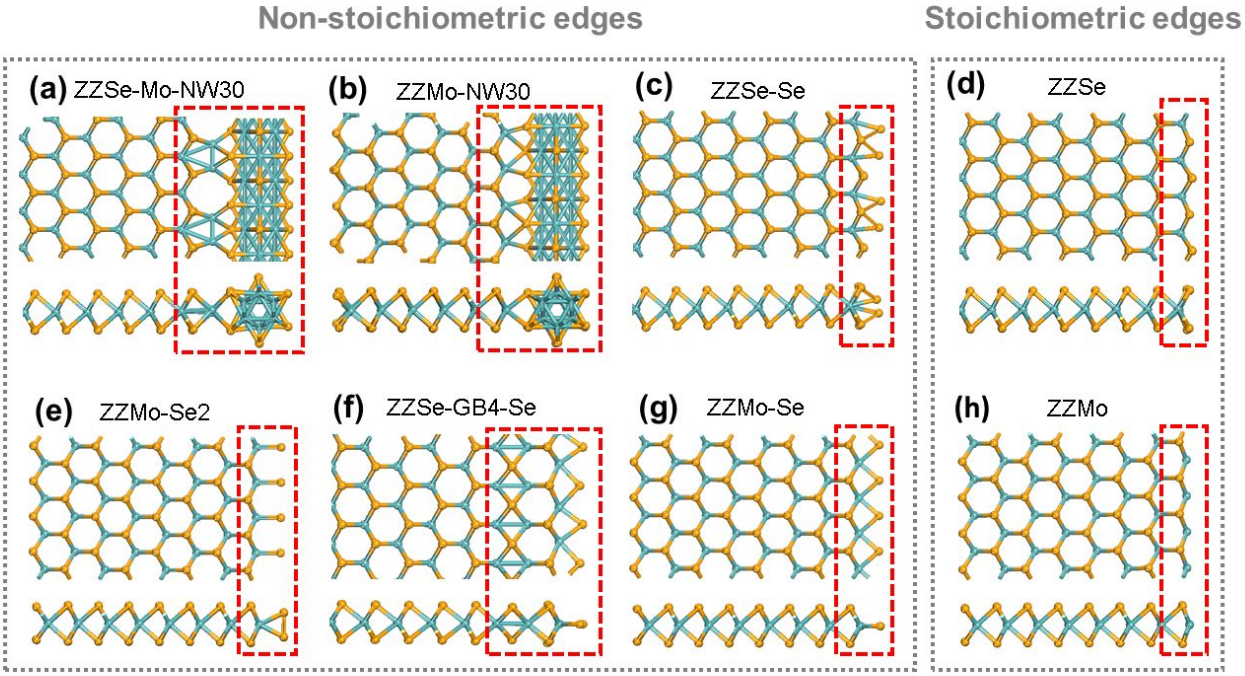

Fig. 1 Top and side views of the six non-stoichiometric and two conventional stoichiometric edges. (a) ZZSe-Mo-NW30. (b) ZZMo-NW30. (c) ZZSe-Se. (d) ZZSe. (e) ZZMo-Se2. (f) ZZSe-GB4-Se. (g) ZZMo-Se. (h) ZZMo. Mo, cyan; Se, orange; H, blue.

Since H adsorption is the first step of HER,[28-30] and the Gibbs free energy for hydrogen adsorption (ΔG_H) is a well-established descriptor for HER,[23] we examine H adsorption at the six non-stoichiometric edges and two stoichiometric edges by calculating ΔG_H. We start with two edges containing nanowire (ZZSe-Mo-NW30 and ZZMo-NW30), followed by two Se-oriented edges (ZZSe-Se and ZZSe), and four Mo-oriented edges (ZZMo-Se2, ZZSe-GB4-Se, ZZMo-Se, and ZZMo). ZZSe-GB4-Se is considered to be Mo-oriented because the boundary near the edge reverses the orientation. Fig. 2 shows the top and side views of the lowest ΔG_H configuration for H adsorption at the six non-stoichiometric and two stoichiometric edges. The other H adsorption structures are shown in Fig. S1.

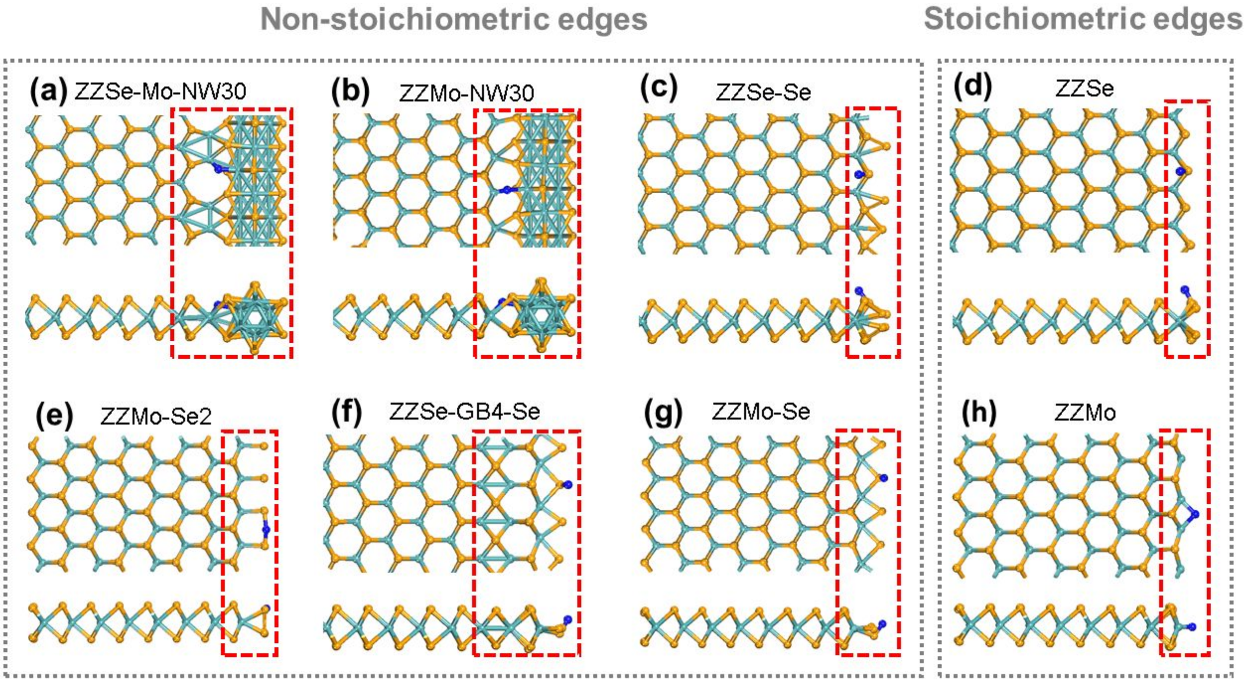

Fig. 2 Top and side views of the lowest ΔG_H configuration for H adsorption at the six non-stoichiometric and two stoichiometric edges. (a) ZZSe-Mo-NW30. (b) ZZMo-NW30. (c) ZZSe-Se. (d) ZZSe. (e) ZZMo-Se2. (f) ZZSe-GB4-Se. (g) ZZMo-Se. (h) ZZMo. Mo, cyan; Se, orange; H, blue.

Edges containing nanowires: We find that H prefers to adsorb at the interface between the nanowire and the basal plane. For ZZSe-Mo-NW30, ΔG_H is 0.38 eV at the interface, while it is 1.35 eV at the basal plane and 0.92 eV at the nanowire. Similarly for ZZMo-NW30, ΔG_H is 0.17 eV at the interface, while it is 1.39 eV at the basal plane and 1.00 eV at the nanowire. As shown in Fig. 2a and 2b, each H atom is bonded with two Mo atoms at the interface. The H-Mo distances are 1.819Å (left) and 1.935Å (right) in ZZSe-Mo-NW30, and 1.794Å (left) and 1.977Å (right) in ZZMo-NW30.

It is noted that the lattice constant of NW30 is 4.4 Å,[31] while the lattice constant of ZZSe/ZZMo is 3.32 Å. ZZSe-Mo-NW30 and ZZMo-NW30 edges are constructed with 1x4 ZZSe/ZZMo and 1x3 NW30, so the lattice mismatch is 0.6%. Since the lattice mismatch is very small, it is expected that the strain effect in ZZSe-Mo-NW30 and ZZMo-NW30 can be neglected. To confirm this hypothesis, we have optimized the lattice constants for ZZSe-Mo-NW30 and ZZMo-NW30 (the lattice constant of 3.32 Å was used before). We find that the optimal lattice constants for ZZSe-Mo-NW30 and ZZMo-NW30 are 3.29 Å and 3.30 Å, respectively. Furthermore, we find that ΔG_H on ZZSe-Mo-NW30 and ZZMo-NW30 with the optimal lattice constants increased only by 0.01 eV. Therefore, we conclude that the strain effect for ZZSe-Mo-NW30 and ZZMo-NW30 is very tiny and can be neglected.

Se-oriented edges: We consider one non-stoichiometric (ZZSe-Se) and one stoichiometric (ZZSe). We find that H is adsorbed at the edge Se site for both of them (Fig. 2c and 2d). The H-Se distance is 1.505 Å in ZZSe-Se and 1.508 Å in ZZSe. ZZSe-Se has a ΔG_H of 0.07 eV, which is very close to zero and suggests it is an excellent HER catalyst, while ZZSe has a more negative ΔG_H of -0.14 eV. This indicates that higher Se coverage at the ZZSe edge can weaken H adsorption and be used to tune HER activity.

Mo-oriented edges: We consider the three non-stoichiometric (ZZMo-Se2, ZZSe-GB4-Se, and ZZMo-Se) and one stoichiometric (ZZMo). For the non-stoichiometric edges, H atoms are all adsorbed at the edge Se sites (Fig. 2e, 2f and 2g). H is bonded with two edge Se in ZZMo-Se2 with H-Se distances of 1.677 Å and 1.872 Å, while H is bonded with one edge Se in ZZ-Se-GB4-Se and ZZMo-Se, both with H-Se distance of 1.494 Å. For the stoichiometric ZZMo edge, H is bonded with two Mo (Fig. 2h), and the H-Mo distance is 1.904 Å. The computed ΔG_H is 0.49 eV for ZZMo-Se2, but it decreases to 0.08 eV for ZZMo-Se, and further decreases to -0.79 eV for ZZMo. This reveals a similar trend as the Se-oriented edges whereby higher Se coverage at the edges can weaken H adsorption. More interestingly, we find that ZZSe-GB4-Se and ZZMo-Se have different ΔG_H, although their structures around the adsorption sites are the same, suggesting that ΔG_H is not only governed by the local adsorption environment.

It is noted that the coordination number of Mo and Se in the basal plane of $MoSe_2$ is six and three, respectively. In ZZSe-Mo-NW30, ZZMo-NW30, and ZZMo, H is bonded to the four/five-coordinated Mo site, while in ZZSe-Se, ZZSe, ZZMo-Se2, ZZSe-GB4-Se, ZZMo-Se, H is bonded to the two-coordinated Se site. Therefore, H always prefers to bond to the under-coordinated sites, irrespective of being Se or Mo, as these sites are more active.

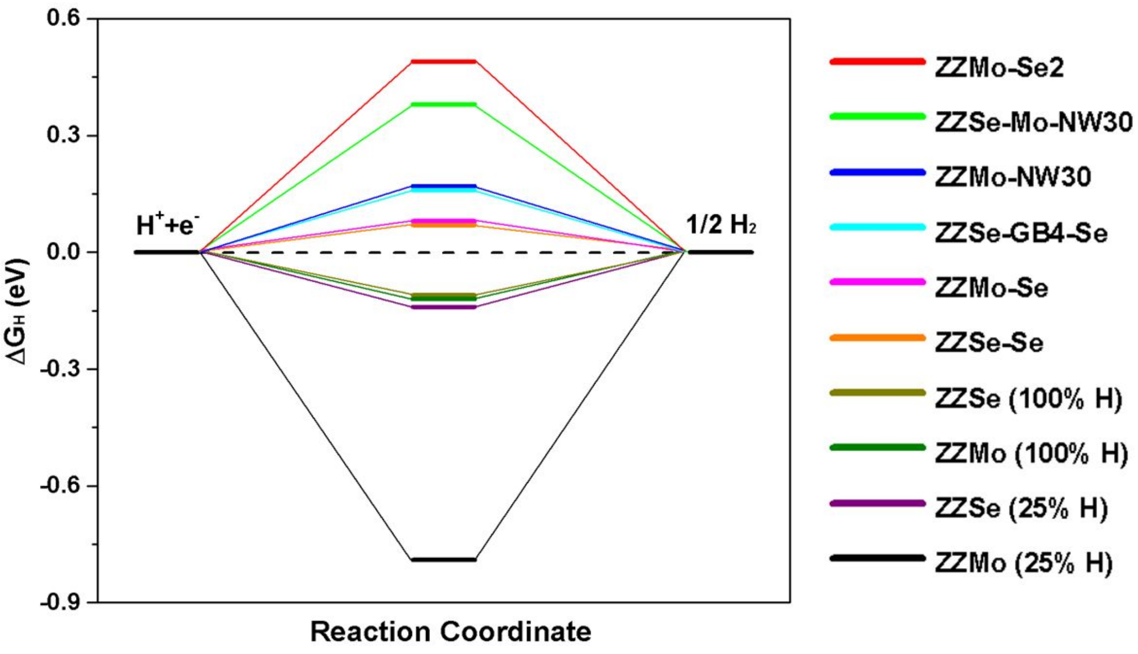

Fig. 3 Calculated free energy diagram for hydrogen evolution of the six non-stoichiometric edges and two stoichiometric edges. For the stoichiometric edges, ΔG_H at different H coverage is shown. The H coverage is defined by n_H/n_{site}, where n_H is the number of adsorbed H, and n_{site} is total number of equivalent adsorption site.

Fig. 3 shows the computed ΔG_H for the six non-stoichiometric edges and two stoichiometric edges. Since a close-to-zero value of ΔG_H suggests a good HER catalyst, we predict four non-stoichiometric edges (ZZMo-NW30, ZZSe-GB4-Se, ZZMo-Se, and ZZSe-Se) to be good HER catalysts (the absolute values of ΔG_H for these edges are within 0.2 eV). However, for the other two non-stoichiometric edges (ZZMo-Se2 and ZZSe-Mo-NW30), their ΔG_H values are very high (0.49 eV and 0.38 eV), suggesting they are inactive for HER. We have also investigated H coverage effect on ΔG_H for the six non-stoichiometric edges. The adsorption free energies and adsorption structures at 50% H coverage are shown in Fig. S2. As one can see, compared to 25% H coverage, ΔG_H increases by 0.10-0.25 eV at 50% H coverage. This indicates that increasing H coverage will weaken H adsorption on the non-stoichiometric edges, which is similar to the stoichiometric edges. Therefore, it is not possible for the six non-stoichiometric edges to adsorb more H (ΔG_H is very positive at high H coverage), and HER at the six non-stoichiometric edges most likely occurs at low H coverage (ΔG_H is close to zero at low H coverage). The stoichiometric edges do not possess close-to-zero ΔG_H at 25% H coverage. By adding more H, we find that, at 100% H coverage, ΔG_H is -0.12 eV for ZZMo and -0.11 eV for ZZSe. Our results on the stoichiometric edges are in agreement with previous studies.[24, 32] Specifically, we discover that certain non-stoichiometric edges could be better HER catalysts than the best-known stoichiometric edges. A recent experimental study is also in apparent agreement that the reconstructed non-stoichiometric MoS_2 edges can be very active for HER.[27] We have also compared our results on the non-stoichiometric $MoSe_2$ edges with other 2D materials (Table S1), and it shows that the ZZSe-Se edge is one of the best 2D electrocatalysts for HER.

To more directly compare the HER activities of the non-stoichiometric ZZSe-Se edge and the stoichiometric ZZSe edge, we have calculated the exchange current densities (i_0). The exchange current density reflects the intrinsic rate of proton transfer from the solvent to the catalytic surface.[23] We find that i_0 of ZZSe-Se and ZZSe is 3.00×10^{-17}A/site and 4.59×10^{-19} A/site, respectively, which shows a difference of two orders of magnitude. Although the difference is not dramatic for now, in the following paragraph we'll show that there are many potential non-stoichiometric $MoSe_2$ edges which can achieve the optimal HER performance, while the stoichiometric edges cannot.

The origin of the high HER activities of the reconstructed non-stoichiometric edges.

In the following section, we will explain why certain non-stoichiometric edges are better for HER catalysis than others by revealing the origin of the high HER activities of the edges. We focus on three effects which we have found to significantly influence ΔG_H: (1) formation of the H–Se/Mo chemical bonds; (2) geometric reconstructions of the edges after H adsorption; and (3) charge redistributions (long-range) of the edges after H adsorption.

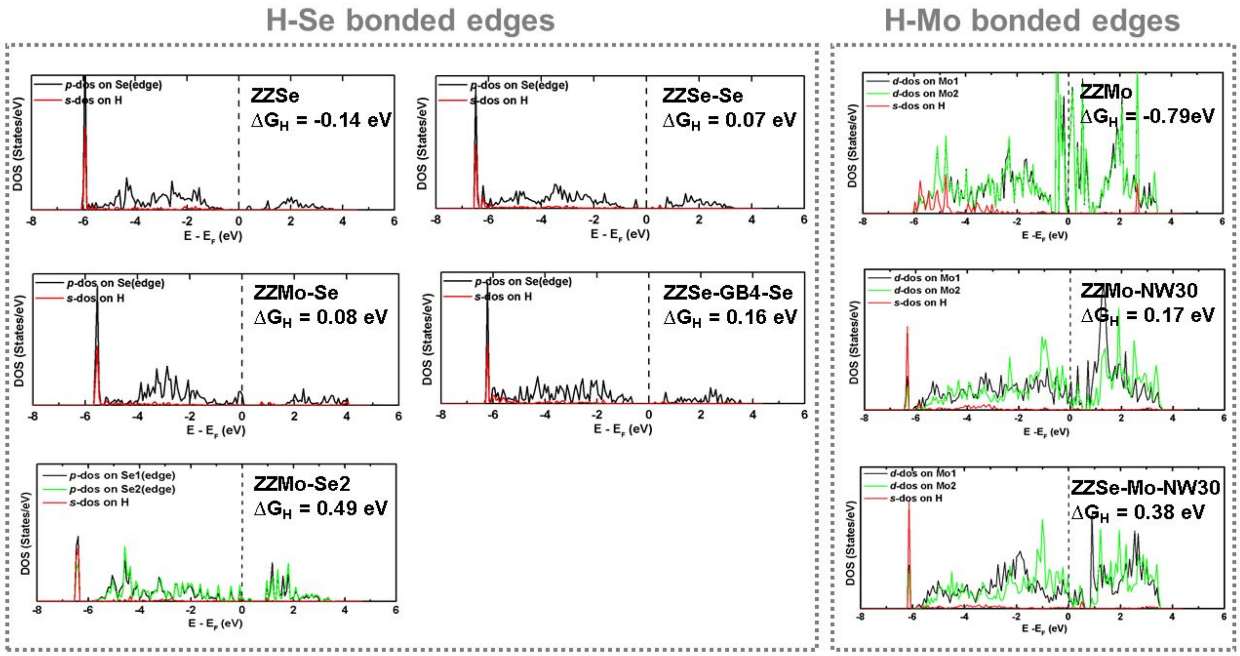

Fig. 4 Projected density-of-states (DOS) for the five H-Se bonded edges and three H-Mo bonded edges. The black and green lines indicate *d/p*-dos of Mo/Se, and the red lines indicate *s*-dos of H.

Formation of the H–Se/Mo chemical bonds: After hydrogen adsorption, the edges can be divided into two groups: H-Se bonded and H-Mo bonded. Fig. 4 shows that for the H-Se bonded edges H adsorption is mainly arises from the interaction of *p*-dos of Se and *s*-dos of H, while for the H-Mo bonded edges H adsorption comes mainly from the interaction of *d*-dos of Mo and *s*-dos of H. However, the overlap areas of the *p*-dos of Se and *s*-dos of H for the five H-Se bonded edges are very similar, although their ΔG_H are different (ranging from -0.14 eV to 0.49 eV). Likewise, the overlap areas of the *d*-dos of Mo and *s*-dos of H for the two H-Mo bonded edges (except ZZMo) are similar. This suggests that the H-Se bond strength in the five H-Se bonded edges, and the H-Mo bond strength in the two H-Mo bonded edges are close. To verify this quantitatively, we compute the integrated crystal orbital Hamilton population (ICOHP) for the H-Se/Mo bonds.[33-35] COHP is a product of the DOS and the overlap Hamiltonian element, and with COHP, the chemistry of bonding–antibonding interactions can be revealed.[33] Indeed, we find that the values of ICOHP are very close (-2.89 eV to -2.68 eV) for the five H-Se bonded edges, and are the same (-1.69 eV) for the two H-Mo bonded edges. Fig. 5 clearly shows that the trend of ΔG_H does not follow the trend of ICOHP. Normally, a more negative ICOHP indicates stronger bond strength. The values of ICOHP in Fig. 5 have been shifted up by 2.26 eV to have the same reference as ΔG_H. 2.26 eV is the energy difference between atomic H and ½ H_2. This suggests that the covalent bonding energy is not the only contributing factor for ΔG_H, as previously hypothesized in stoichiometric-edges.[24]

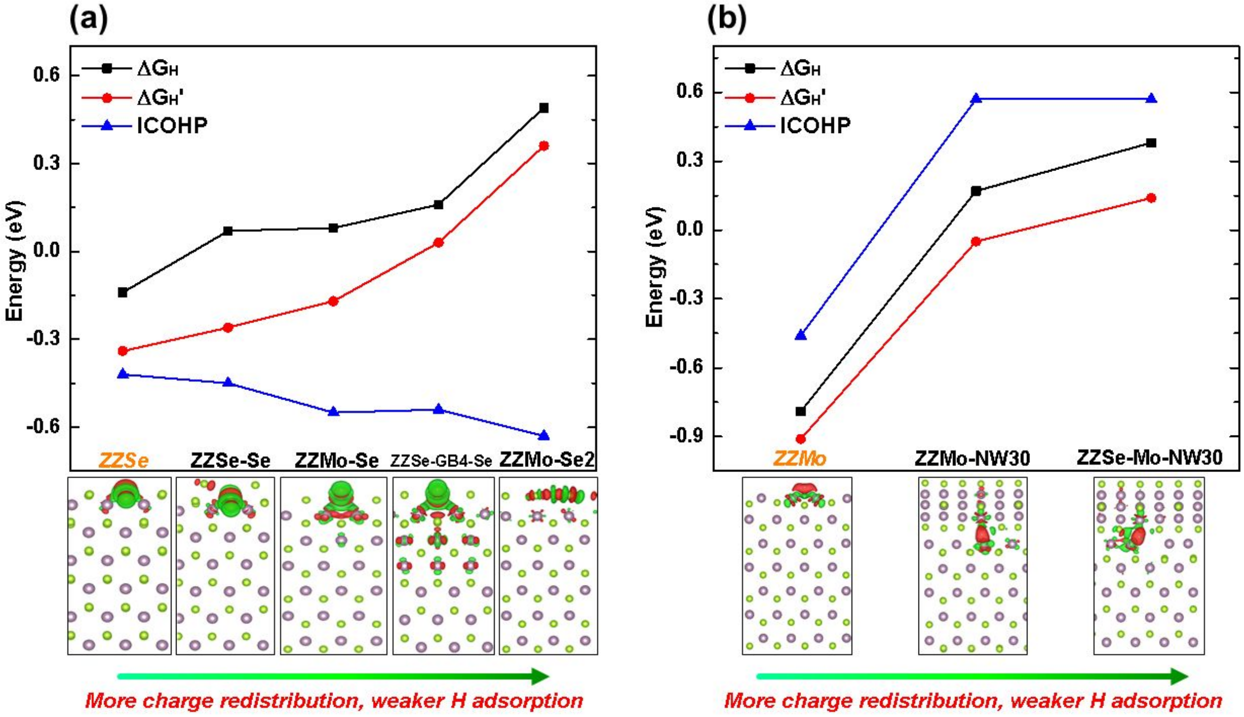

Fig. 5 ΔG_H, ΔG_H', ICOHP (shifted up by 2.26 eV), and charge density difference plots for the five H-Se bonded edges (a) and three H-Mo bonded edges (b). The stoichiometric edges are labeled in orange. The red color in the charge density difference plots indicates charge accumulation and the green color indicates charge depletion. The value of the isosurface is 0.002 eV/Å^3. Se, green; Mo, grey; H, white.

Geometric reconstructions: We have noticed geometric reconstructions at the edges after H adsorption, and these reconstructions can contribute to ΔG_H,[36-38] and we compute Gibbs free energies of hydrogen adsorption which are referenced to the edge structures after H adsorption (ΔG_H'). In other words, ΔG_H' has the energetic contribution for the geometric reconstructions of the edges after H adsorption, removed from ΔG_H. Table 1 lists ΔG_H, ΔG_H', and their difference $\Delta\Delta G_H$ (ΔG_H-ΔG_H') for the five H-Se bonded edges and three H-Mo bonded edges (the stoichiometric edges are labeled in orange). One can see that the values of $\Delta\Delta G_H$ range from 0.12 eV to 0.33 eV, confirming that geometric reconstructions certainty contribute to ΔG_H. It also shows that the magnitudes of geometric reconstructions of the edges are different. However even with the energetic cost for geometric reconstructions removed, the trend of ΔG_H' doesn't follow the trend of ICOHP (Fig. 5), For example, ZZMo-Se and ZZSe-GB4-Se have almost the same ICOHP, but their difference in ΔG_H' is 0.20 eV. This suggests that some other factor is affecting ΔG_H'.

Table 2 Gibbs free energies of hydrogen adsorption which are referenced to the edge structures before H adsorption (ΔG_H) and after H adsorption (ΔG_H') for the five H-Se bonded edges and three H-Mo bonded edges. The stoichiometric edges are labeled in orange. The difference between ΔG_H and ΔG_H' ($\Delta\Delta G_H$) is also shown.

	ZZSe	**ZZSe-Se**	**ZZMo-Se**	**ZZ-Se-GB4-Se**	**ZZMo-Se2**	***ZZMo***	**ZZMo-NW30**	**ZZSe-Mo-NW30**
ΔG_H / eV	*-0.14*	0.07	0.08	0.16	0.49	*-0.79*	0.17	0.38
ΔG_H' / eV	*-0.34*	-0.26	-0.17	0.03	0.36	*-0.91*	-0.05	0.14
$\Delta\Delta G_H$ / eV	*0.20*	0.33	0.25	0.13	0.13	*0.12*	0.22	0.24

Charge redistributions: To understand if there is any underlying electronic-structure derived quantity that explains the observed differences in ΔG_H', we plotted the charge density difference isosurfaces of the edges before and after H adsorption (Fig. 5 lower panel). Surprisingly, we find that the change density differences are very different for ZZMo-Se and ZZSe-GB4-Se, even though the coordination around the H adsorption site look similar. The plane-averaged charge density difference plots (Fig. 6) clearly shows charge accumulations at the grain boundary in ZZSe-GB4-Se. Therefore, the difference in ΔG_H' for ZZSe-GB4-Se and ZZMo-Se can be explained by their difference in charge redistribution after H adsorption. Similarly, the difference in ΔG_H' for ZZSe *vs.* ZZSe-Se, and ZZSe-Mo-NW30 *vs.* ZZMo-NW30 can be explained by the same manner.

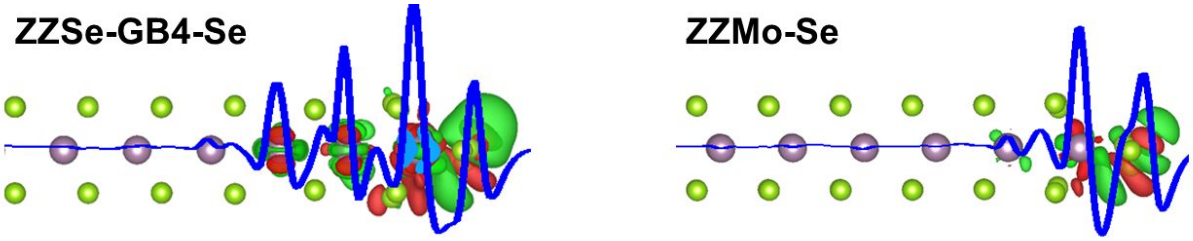

Fig. 6 Plane-averaged charge density difference for ZZSe-GB4-Se and ZZMo-Se.

Design principles for tuning the HER activities of non-stoichiometric edges

We have showed that ΔG_H is a combined result of chemical bond formation, geometric reconstruction, and charge redistribution of the edges after H adsorption, so ΔG_H cannot simply be predicted by the conventional descriptors such as the *d*/*p*-band centers,[24, 39, 40] as these descriptors are only related to the formation of the chemical bonds. Our next question is if we can find any electronic structure property that correlates with ΔG_H. This could provide a valuable design principle for tuning these non-stoichiometric edges, leading to further improvement in the HER performance.

The charge density difference plots in Fig. 5 suggests that the more charge is localized on H (i.e. less is the charge redistribution), the stronger the H adsorption. Since charge-redistribution will affect the amount of charge in the Wigner-Seitz cell around H (i.e. the Bader-charge), we calculated Bader charges on H at many different adsorption sites for each edge to quantify the effect of charge-redistribution, and tried to see if they correlate with ΔG_H. As shown in Fig. 7, for the same type of edge (H-Se bonded or H-Mo bonded), ΔG_H has a strong linear correlation with the Bader charge on H, and the more negative the Bader charge on the adsorbed H, the stronger the H adsorption. Due to the smaller electronegativity of Mo (2.16) than Se (2.55), Bader charges on H in H-Mo bonded edges are more negative than H-Se bonded edges. This correlation can explain our previous observations of high Se coverages at the edges giving rise to weak H adsorption. The electronegativity of Se is higher than H (2.20), so the electrons can be withdrawn from H at high Se coverages and lead to weak H adsorption.

Based on the linear correlation, we compute the optimal charges on H for HER ($\Delta G_H = 0$). We find that the optimal charge is -0.0675 |e| for H adsorbed at the Se sites, and -0.3322|e| for H adsorbed at the Mo sites. It is noted that the optimal charges are not obtained in the stoichiometric edges, but can be realistically achieved by controlling the chemical environment (μ_{Mo}) to create non-stoichiometric edges possessing tunable Mo/Se ratios, such as different Se coverages at ZZSe/ZZMo, nanowire, grain boundary, etc. In addition, the optimal charges are all negative, which will promote the next step of HER *via* the Heyrovsky mechanism: $H_{ad} + H^+ + e^- \rightarrow H_2$.[29]

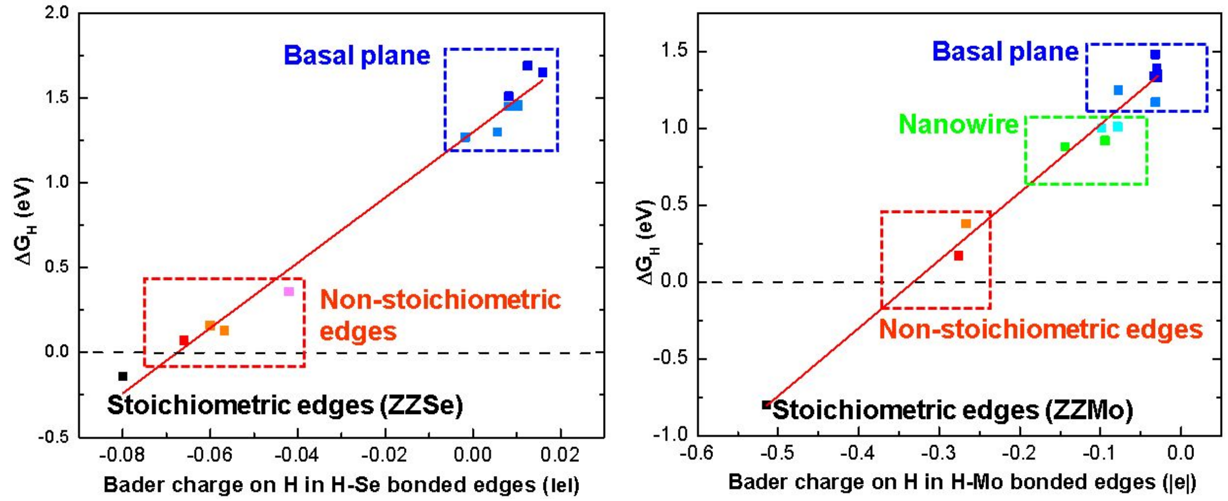

Fig. 7 Linear correlation of Bader charges on H and ΔG_H in H-Se bonded edges (left) and H-Mo bonded edges (right). The dash line indicates ΔG_H of zero.

Conclusions

In conclusion, we have investigated if tuning the non-stoichiometric degree of the $MoSe_2$ edges can improve their HER activities. We find that the non-stoichiometric edges can have even better HER performance than the conventional stoichiometric edges (ZZSe and ZZMo). We demonstrate that the high HER activities are not only attributed to the formation of the H-Se/Mo chemical bonds, but also governed by geometric reconstructions and charge redistributions (long-range) of the edges after H adsorption. More excitingly, we find a linear correlation between ΔG_H and Bader charges on H, and based on this linear correlation, we get the optimal charges on H for HER. The optimal charges cannot be obtained in the stoichiometric edges, but can be realistically achieved by controlling the chemical environment (μ_{Mo}) to create non-stoichiometric edges possessing tunable Mo/Se ratios. Our study opens the door for chemistry-driven engineering of non-stoichiometric 2D TMDC edges for superior HER performance.

Computational methods

Spin-polarized density functional theory (DFT) calculations were performed using the Vienna *ab initio* simulation package (VASP).[41, 42] Electron exchange-correlation was represented by the functional of Perdew, Burke and Ernzerhof (PBE) of generalized gradient approximation (GGA).[43] The ion-electron interaction was described with the projector augmented wave (PAW) method.[44] The plane-wave cutoff is set to 400 eV, and a conjugate gradient method is applied to relax the geometry until interatomic forces are less than 0.025 eV/Å. The Brillouin zone was sampled using a 1 × 3 × 1 Monkhorst-Pack k-point meshes for the 1 × 4 supercells. The calculated lattice constant of 3.32 Å for the $MoSe_2$ monolayer is used to set up the supercells. Vacuum spaces in x and z directions are larger than 10 Å. Partial atomic charges were obtained using Bader charge analysis as implemented by Henkelman and co-workers.[45] Charge density difference isosurfaces were visualized using the VESTA program.[46]

The edge free energy γ was calculated by

$$\gamma = \frac{1}{2L}[E(edge) - N_{Mo}E(MoSe_2) + (2N_M - N_{Se})\mu_{Se}] \quad (1)$$

where L is the length of the edge in the unit cell, E(edge) is the total energy of the edges, N_{Mo} is the number of Mo, $E(MoSe_2)$ is the energy per formula unit of $MoSe_2$ monolayer, N_{Se} is the number of Se, and μ_{Se} is the chemical potential of Se.[22] The chemical potential of Se was determined by the following equilibrium reactions

$$2(H^+ + e^-) + Se(*) \leftrightarrow H_2Se + (*) \quad (2)$$

and

$$H^+ + e^- \leftrightarrow H \quad (3)$$

where (*) denotes a selenide vacancy on the edge. Using the computational hydrogen electrode,[23] μ_{Se} can be determined by

$$\mu_{Se} = \mu_{H2Se} - 2(\frac{1}{2}\mu_{H2} - eU_{RHE}) \quad (4)$$

where U_{RHE} is the potential versus the reversible hydrogen electrode. The potential was assumed to be U = 0 V_{RHE} because we are interested in the region of low overpotential. Due to the negligible pressure of H_2Se under reaction conditions, μ_{Se} is expected to be extremely negative.[24]

The differential H adsorption energy ΔE_H was calculated by

$$\Delta E_H = E(\text{catalyst} + H) - E(\text{catalyst}) - 1/2E(H_2) \quad (5)$$

where E(catalyst + H) represents the total energy of the catalyst with one adsorbed H atom, E(catalyst) represents the total energy of the catalyst, and $E(H_2)$ represents the total energy of a gas phase H_2 molecule. A negative value of ΔE_H suggests favorable absorption. The Gibbs free energy of H adsorption ΔG_H was obtained by

$$\Delta G_H = \Delta E_H + \Delta E_{ZPE} - T\Delta S_H \quad (6)$$

where ΔE_{ZPE} is the difference in zero-point energy between the adsorbed H and H in the gas phase H_2 molecule, and ΔS_H is the entropy difference between the adsorbed H and ½ H_2 in the gas phase under standard conditions. The zero-point energy was calculated by summing vibrational frequencies ω over normal modes ν: $E_{ZPE} = \frac{1}{2}\sum \hbar\omega$. The entropy of the free H_2 molecule at 298.15 K and 1 atm was taken from the NIST database.[47]

If the proton transfer is exothermic ($\Delta G_H < 0$), the exchange current densities i_0 was expressed as

$$i_0 = -ek_0 \frac{1}{1 + \exp(-\Delta G_H/kT)} \quad (7)$$

where k_0 is the rate constant (k_0 = 200 s^{-1} $site^{-1}$) which includes all effects relating to the reorganization of the solvent during the proton transfer to the catalytic surface, and k is the Boltzmann constant.[23] The hydrogen evolution was evaluated as standard conditions corresponding to pH = 0 with T = 300 K. If the proton transfer is endothermic ($\Delta G_H > 0$), i_0 was expressed as

$$i_0 = -ek_0 \frac{1}{1 + \exp(-\Delta G_H/kT)} \exp(-\Delta G_H/kT). \quad (8)$$

Acknowledgements

This research was supported by an ORNL LDRD program. A portion of this research was conducted at the Center for Nanophase Materials Sciences, which is a DOE Office of Science User Facility. This research used resources of the National Energy Research Scientific Computing Center, a DOE Office of Science User Facility supported by the Office of Science of the U.S. Department of Energy.

References

1 W. Lubitz and W. Tumas, *Chem. Rev.*, 2007, **107**, 3900-3903.

2 Y. Zheng, Y. Jiao, M. Jaroniec and S. Z. Qiao, *Angew. Chem. Int. Ed.*, 2015, **54**, 52-65.

3 P. Liu and J. A. Rodriguez, *J. Am. Chem. Soc.*, 2005, **127**, 14871-14878.

4 E. J. Popczun, J. R. McKone, C. G. Read, A. J. Biacchi, A. M. Wiltrout, N. S. Lewis and R. E. Schaak, *J. Am. Chem. Soc.*, 2013, **135**, 9267-9270.

5 E. J. Popczun, C. G. Read, C. W. Roske, N. S. Lewis and R. E. Schaak, *Angew. Chem. Int. Ed.*, 2014, **53**, 5427-5430.

6 G. Hu, Q. Tang and D. E. Jiang, *Phys. Chem. Chem. Phys.*, 2016, **18**, 23864-23871.

7 B. You, X. Liu, G. Hu, S. Gul, J. Yano, D. E. Jiang and Y. Sun, *J. Am. Chem. Soc.*, 2017, **139**, 12283-12290.

8 Y. Li, H. Wang, L. Xie, Y. Liang, G. Hong and H. Dai, *J. Am. Chem. Soc.*, 2011, **133**, 7296-7299.

9 D. Voiry, M. Salehi, R. Silva, T. Fujita, M. Chen, T. Asefa, V. B. Shenoy, G. Eda and M. Chhowalla, *Nano Lett.*, 2013, **13**, 6222-6227.

10 D. Voiry, J. Yang and M. Chhowalla, *Adv. Mater.*, 2016, **28**, 6197-6206.

11 D. Kim, J. Shi and Y. Liu, *J. Am. Chem. Soc.*, 2018, **140**, 9127-9131.

12 S. Park, J. Park, H. Abroshan, L. Zhang, J. K. Kim, J. Zhang, J. Guo, S. Siahrostami and X. Zheng, *ACS Energy Lett.*, 2018, **3**, 2685-2693.

13 B. Hinnemann, P. G. Moses, J. Bonde, K. P. Jørgensen, J. H. Nielsen, S. Horch, I. Chorkendorff and J. K. Nørskov, *J. Am. Chem. Soc.*, 2005, **127**, 5308-5309.

14 T. F. Jaramillo, K. P. Jørgensen, J. Bonde, J. H. Nielsen, S. Horch and I. Chorkendorff, *Science*, 2007, **317**, 100-102.

15 Q. Gong, L. Cheng, C. Liu, M. Zhang, Q. Feng, H. Ye, M. Zeng, L. Xie, Z. Liu and Y. Li, *ACS Catal.*, 2015, **5**, 2213-2219.

16 H. Wang, C. Tsai, D. Kong, K. Chan, F. Abild-Pedersen, J. K. Nørskov and Y. Cui, *Nano Res.*, 2015, **8**, 566-575.

17 L. Wu, X. Xu, Y. Zhao, K. Zhang, Y. Sun, T. Wang, Y. Wang, W. Zhong and Y. Du, *Appl. Surf. Sci.*, 2017, **425**, 470-477.

18 W. Xiao, P. Liu, J. Zhang, W. Song, Y. P. Feng, D. Gao and J. Ding, *Adv. Energy Mater.*, 2017, **7**, 1602086.

19 X. Huang, M. Leng, W. Xiao, M. Li, J. Ding, T. L. Tan, W. S. V. Lee and J. Xue, *Adv. Funct. Mater.*, 2017, **27**, 1604943.

20 D. Gao, B. Xia, C. Zhu, Y. Du, P. Xi, D. Xue, J. Ding and J. Wang, *J. Mater. Chem. A*, 2018, **6**, 510-515.

21 X. Sang, X. Li, W. Zhao, J. Dong, C. M. Rouleau, D. B. Geohegan, F. Ding, K. Xiao and R. R. Unocic, *Nat. Commun.*, 2018, **9**, 2051.

22 M. Bollinger, K. W. Jacobsen and J. K. Nørskov, *Phys. Rev. B*, 2003, **67**, 085410.

23 J. K. Nørskov, T. Bligaard, A. Logadottir, J. R. Kitchin, J. G. Chen, S. Pandelov and U. Stimming, *J. Electrochem. Soc.*, 2005, **152**, J23-J26.

24 C. Tsai, K. Chan, F. Abild-Pedersen and J. K. Nørskov, *Phys. Chem. Chem. Phys.*, 2014, **16**, 13156-13164.

25 W. Zhou, X. Zou, S. Najmaei, Z. Liu, Y. Shi, J. Kong, J. Lou, P. M. Ajayan, B. I. Yakobson and J.-C. Idrobo, *Nano Lett.*, 2013, **13**, 2615-2622.

26 D. Cao, T. Shen, P. Liang, X. Chen and H. Shu, *J. Phys. Chem. C*, 2015, **119**, 4294-4301.

27 X. Zhao, D. Fu, Z. Ding, Y. Y. Zhang, D. Wan, S. J. Tan, Z. Chen, K. Leng, J. Dan and W. Fu, *Nano Lett.*, 2017, **18**, 482-490.

28 T. Erdey-Gruz and M. Volmer, *Z. Phys. Chem. A*, 1930, **150**, 203.

29 J. Heyrovský, *Recl. Trav. Chim. Pays-Bas*, 1927, **46**, 582-585.

30 J. Tafel, *Z. phys. Chem*, 1905, **50**, 641.

31 J. Lin, O. Cretu, W. Zhou, K. Suenaga, D. Prasai, K. I. Bolotin, N. T. Cuong, M. Otani, S. Okada and A. R. Lupini, *Nat. Nanotechnol.*, 2014, **9**, 436.

32 R. Kronberg, M. Hakala, N. Holmberg and K. Laasonen, *Phys. Chem. Chem. Phys.*, 2017, **19**, 16231-16241.

33 R. Dronskowski and P. E. Blöchl, *J. Phys. Chem.*, 1993, **97**, 8617-8624.

34 V. L. Deringer, A. L. Tchougréeff and R. Dronskowski, *J. Phys. Chem. A*, 2011, **115**, 5461-5466.

35 S. Maintz, V. L. Deringer, A. L. Tchougréeff and R. Dronskowski, *J. Comput. Chem.*, 2016, **37**, 1030-1035.

36 J. Balachandran, L. Lin, J. S. Anchell, C. A. Bridges and P. Ganesh, *J. Phys. Chem. C*, 2017, **121**, 26637-26647.

37 J. Ding, J. Balachandran, X. Sang, W. Guo, G. M. Veith, C. A. Bridges, C. M. Rouleau, J. D. Poplawsky, N. Bassiri-Gharb and P. Ganesh, *ACS Appl. Mater. Interfaces*, 2018, **10**, 4816-4823.

38 J. Ding, J. Balachandran, X. Sang, W. Guo, J. S. Anchell, G. M. Veith, C. A. Bridges, Y. Cheng, C. M. Rouleau and J. D. Poplawsky, *Chem. Mater.*, 2018, **30**, 4919-4925.

39 J. Greeley, J. K. Nørskov and M. Mavrikakis, *Annu. Rev. Phys. Chem.*, 2002, **53**, 319-348.

40 J. Kitchin, J. K. Nørskov, M. Barteau and J. Chen, *J. Chem. Phys.*, 2004, **120**, 10240-10246.

41 G. Kresse and J. Furthmüller, *Phys. Rev. B*, 1996, **54**, 11169-11186.

42 G. Kresse and J. Furthmüller, *Comput. Mater. Sci.*, 1996, **6**, 15-50.

43 J. P. Perdew, K. Burke and M. Ernzerhof, *Phys. Rev. Lett.* , 1996, **77**, 3865-3868.

44 P. E. Blöchl, *Phys. Rev. B*, 1994, **50**, 17953-17979.

45 W. Tang, E. Sanville and G. Henkelman, *J. Phys. Condens. Matter*, 2009, **21**, 084204.

46 K. Momma and F. Izumi, *J. Appl. Crystallogr.*, 2011, **44**, 1272-1276.

47 P. J. Linstrom and W. Mallard, 2001.

TOC Graphic

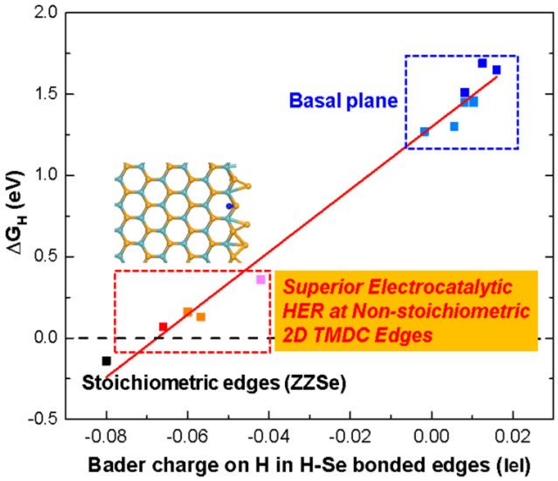
2.0
1.5
1.0
0.5
0.0
-0.5
ΔG_H (eV)
Basal plane
Superior Electrocatalytic HER at Non-stoichiometric 2D TMDC Edges
Stoichiometric edges (ZZSe)
-0.08
-0.06
-0.04
-0.02
0.00
0.02
Bader charge on H in H-Se bonded edges (|e|)